Vapour-Liquid Equilibria for Carbon Dioxide (CO_2) + 3,3,3-Trifluoropropene (HFO-1243zf) Binary Mixtures at Temperatures between (288 and 348) K

Mirhadi S. Sadaghiani[1], Arash Arami-Niya[1, 2], Benjamin Marsh[1], Saif Al Ghafri[1], Eric F. May[*1]

[1] *Fluid Science & Resources Division, Department of Chemical Engineering, The University of Western Australia, 35 Stirling Hwy, Crawley 6009, Australia*

[2] *Discipline of Chemical Engineering, Western Australian School of Mines: Minerals, Energy and Chemical Engineering, Curtin University, GPO Box U1987, Perth, WA 6845, Australia*

Table of Contents Graphic (JCED Requirement)

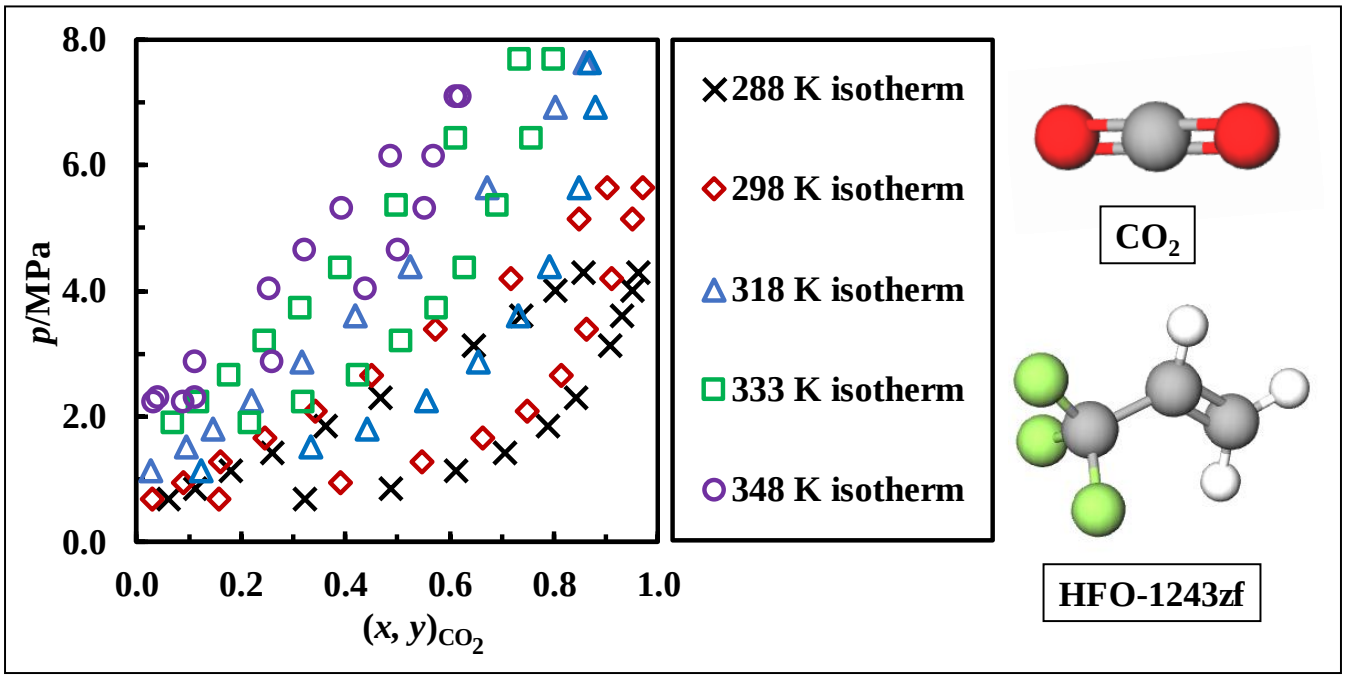

* E-mail addresses: Eric.May@uwa.edu.au

Abstract

Accurate property data for mixtures of hydrofluoroolefins with refrigerants like CO_2 are needed by industry to design safe and efficient refrigeration systems that employ low global warming potential working fluids. However, data available for these mixtures, particularly at conditions of vapour-liquid-equilibrium (VLE), are limited. In this work, the VLE of CO_2 and HFO-1243zf binary mixtures, which has not been studied previously, was measured along five isotherms at temperatures between (288 and 348) K and pressures between (0.68 and 7.69) MPa. The new VLE data are compared with the predictions of a Helmholtz free energy model that utilise GERG-2008 mixing rules. Adjusting the model's binary interaction parameters (BIPs) to force agreement with the new measurements reduced the relative root mean square deviation (RMSD) of the data from the model by 45 % relative to the default BIPs. Additionally, the data were compared with predictions from the Peng Robinson Advanced equation of state (PRA-EOS) with a one-fluid mixing rule and a fixed binary interaction parameter which was subsequently tuned to the experimental data. The tuned PRA-EOS could represent the experimental CO_2 mole fractions with an RMSD of 0.012, which is about three times larger than the average experimental uncertainty, while the RMSD of the tuned Helmholtz free energy model from the experimental data was 0.009. The accurate data and improved model presented in this work will aid the development of environmentally friendly refrigerant mixtures.

Keywords: 3,3,3-Trifluoropropene; HFO-1243zf; Vapour-liquid-equilibrium; Global warming potential; Carbon dioxide.

Introduction

Hydrofluoroolefins (HFOs) are a new generation of refrigerants with much lower global warming potential (GWP) than the commonly used hydrofluorocarbons (HFCs). Three HFOs, namely HFO-1234yf, HFO-1234ze(E) and HFO-1243zf, are in particular excellent candidates to replace HFC-134a, which is widely used in domestic refrigeration systems but has a GWP of around 1300 and atmospheric lifetime of 13 years[1]. Of the three HFOs, HFO-1243zf has the lowest GWP of 0.29 with an atmospheric lifetime of about six days [2]; such a refrigerant could help meet the objectives of the Montreal Protocol [3] and the Kigali Amendment [4].

One barrier to the uptake of HFO replacement is the scarcity of the existing thermophysical property data available for HFOs blends. While the thermophysical properties of HFO-1234yf and HFO-1234ze(E) mixtures have been quite well studied [5–12], limited thermophysical property data are available for mixtures containing HFO-1243zf including its binary systems with HFC-134a [1,13], iso-butane [14] and propane [15]. However, pure HFO-1243zf has demonstrated a higher coefficient of performance when used in an air conditioner than did HFC-134a, HFC-22 and HFC-32 [16]. Despite this potential, the experimental data available for pure HFO-1243zf and its binary mixtures are limited, as shown in Table 1.

In terms of thermophysical properties modelling, Akasaka and Lemmon [17,18] and Bobbo et al. [19] studied the performance of Helmholtz energy equations of state (EOS) for predicting the thermodynamic properties of HFO-1243zf. They showed that Helmholtz energy EOS were able to represent pure HFO-1243zf at temperatures between 234 K and 440 K and pressures up to 34 MPa with estimated uncertainties of 0.1 % for vapour pressure, 0.05 % for liquid density and 0.6% for vapour density.

Table 1: Summary of the open literature of thermodynamic property data for pure HFO-1243zf and its binary mixtures.

System	Properties	Range (T, p, z^*)	Reference
HFO-1243zf	T_c, p_c, ρ_c, ω, c_p	233-292 K, 0.1-10 MPa, pure	[20]
HFO-1243zf	p_{sat}	234-373 K; 0.1-3.2 MPa, pure	[21,22]
HFO-1243zf	p_{sat}	310-375 K, 0.8-3.4 MPa, pure	[23]
HFO-1243zf	p_{sat}	278-377 K, 0.8-4.5 MPa, pure	[24]
HFO-1243zf	pvT	279-368 K; 0.3-0.9 MPa, pure	[25]
HFO-1243zf	ρ_{sat}	240-370 K, Not Reported, pure	[26]
HFO-1243zf + HFC-134a	VLE	293-323 K, 0.5-1.3 MPa, 0-1.00	[1]
HFO-1243zf + HFC-134a	VLE	243-293 K, 0.08-0.5 MPa, 0-1.00	[13]
HFO-1243zf + iso-butane	VLE	253-293 K, 0.07-0.3 MPa, 0-1.00	[14]
HFO-1243zf + propane	VLE	243-288 K, 0.08-0.7 MPa, 0-1.00	[15]
HFO-1243zf + iso-butane	$pvTx$	308-383 K, 0.05-0.4 MPa, 0.1-0.78	[27]

* z represents the mole fraction of the first-named component in the binary mixture (last row only).

On the other hand, HFOs' moderate flammability is another barrier to its widespread applications in domestic refrigeration systems because it may pose safety risks to users [28]. To mitigate this, HFOs can be blended with non-flammable refrigerants like HFC-134a, HFC-125 and carbon dioxide (CO_2) to neutralise their flammability with only minor cooling performance reductions. Carbon dioxide (CO_2) is an easily obtained non-flammable organic refrigerant with low GWP and zero ODP. Mclinden et al. [29] conducted a comprehensive simulation-based study that ranked CO_2 next to HFO-1243zf as two of the most promising 62 refrigerants based on flammability, GWP and thermodynamic parameters. Bell et al. [30] carried out simulations that assessed the best replacements for HFC-134a, selecting HFO-1243zf and CO_2 as key targets of future work.

While data for binary mixtures of CO_2 with HFO-1234yf and HFO-1234ze have been reported [11,31,32], no experimental property data have been measured for the CO_2 + HFO-1243zf binary system. Vapour-liquid-equilibrium (VLE) data are particularly important to the design and optimisation of cooling systems that utilise alternative refrigerants [33]. In this work, we measured the VLE of CO_2 + HFO-1243zf binary system at five isotherms between (288 and

348) K. The analytical method was employed to generate new VLE data with quantitative uncertainty estimates to enable the development of improved models. The experimental setup, materials, calibration and experimental procedures are discussed, and the data are compared with the predictions of two thermodynamics models for the mixture, one based on a Helmholtz free energy EOS and the other on the Peng Robinson Advanced (PRA) EOS. Finally, both models are tuned based on the acquired experimental data, and their performance in properties predictions are compared with the original models.

Experimental

Apparatus

Two identical apparatus sharing one analysis system, as shown in Figure 1 and similar to those described in our previous studies [7,11,34], were used in this work to measure the VLE of the binary mixtures. Previously, this apparatus was used to measure the VLE properties for binary systems of CO_2 + HFC-32, CO_2 + HFC-125, CO_2 + HFC-134a and CO_2 + HFC-1234yf [11], mixtures that were studied in the literature. The measured VLE data were consistent with earlier research by a difference within the estimated uncertainty. This validates the data quality of the VLE properties for CO_2 + HFO-1243zf studied in this work.

Each apparatus consisted of an equilibrium cell machined from a single stainless steel (SAE316L) billet with an internal volume of 65 ml and a pressure rating up to 30 MPa, shown in Figure 2. The outer surfaces of the equilibrium cells were coated with 1 mm thickness of copper to enhance temperature uniformity and heat transfer. A quartz-crystal pressure transducer (Digiquartz, Paroscientific) with a full scale of 13.8 MPa and a relative standard uncertainty of 0.01% of the full scale was used to measure the system's pressure. A magnetic stirrer was placed inside each equilibrium cell and used to ensure the mixture's homogeneity before sampling.

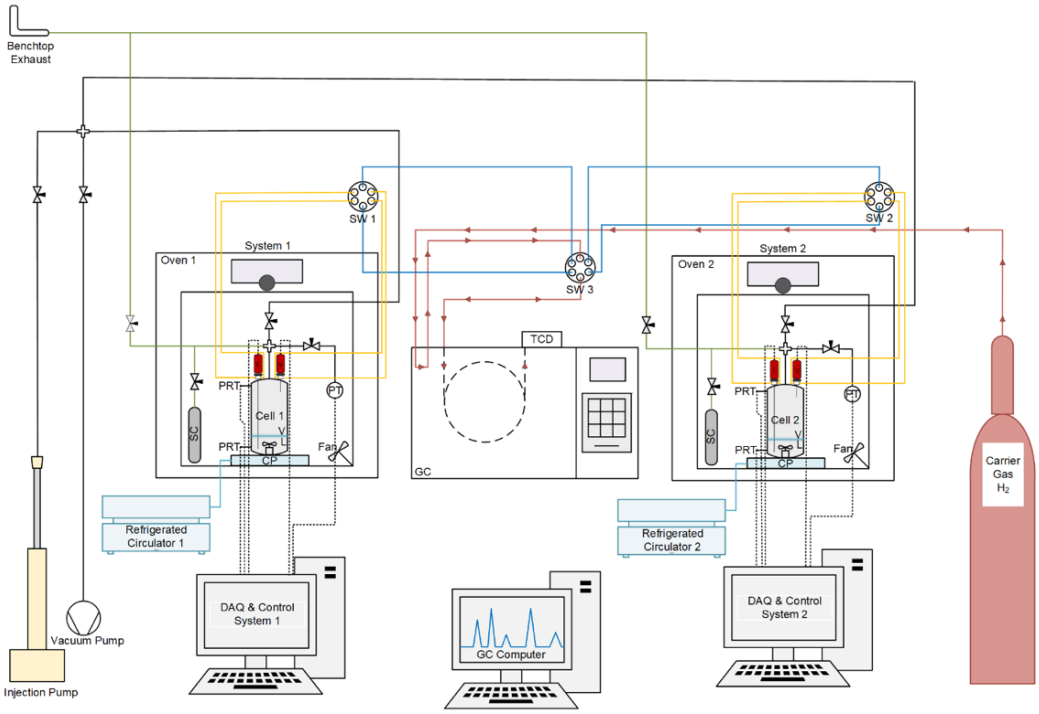

Figure 1: The schematic diagram of the VLE apparatus (CP: Cooling Plate; DAQ: Data Acquisition; GC: Gas Chromatograph, PRT: Platinum Resistance Thermometer; SC: Sample Cylinder; SW*: Switch Valve; TCD: Thermal Conductivity Detector) [11].

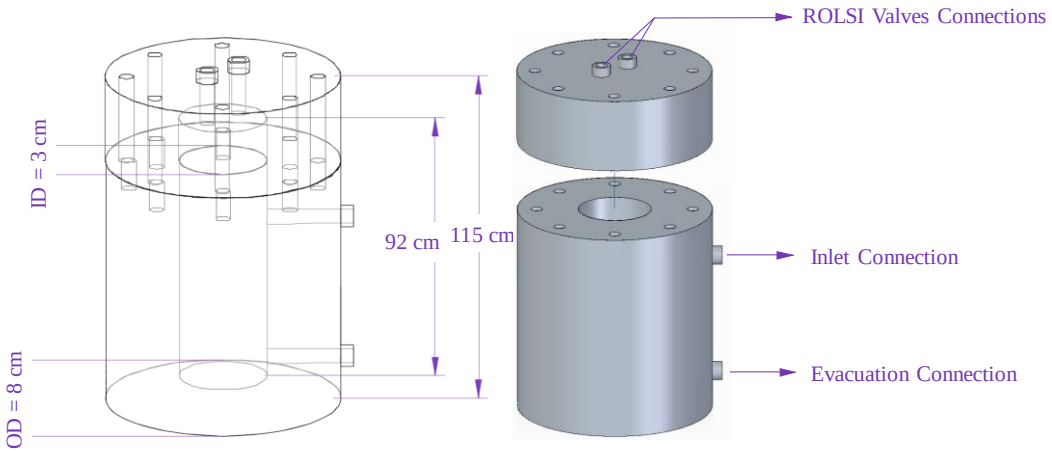

Figure 2: Visualisation showing an exploded view of the equilibrium cell.

Each equilibrium cell was housed inside its own incubator oven (Memmert-UN110) allowing it to be controlled at temperatures between (288 and 348) K with a temperature stability of 0.05 K over the duration of an isothermal VLE experiment (6 to 10 h). Temperatures below ambient were achieved using a custom cooling system consisting of spiral copper tubes-plate

placed inside the oven and connected to refrigerated circulators (PolyScience-9502A12E), similar to the approach taken by Efika et al. [35]. The temperature was monitored using two platinum resistance thermometers (NR-141-100S, Nitsushin) with a standard uncertainty of 0.05 K. These PRTs were calibrated against a standard PRT (ASL-WIKA) in a constant temperature bath between 273.15 K and 398.15 K. The average temperature difference between these PRTs during the VLE measurement was less 0.1 K.

Two remotely controlled electromagnetic sampling (Rapid On-Line Sampling Injectors – ROLSI^{TM}) [36,37] valves were used to sample the vapour and liquid phases. A stainless steel (SAE316L) capillary tube with an ID of 0.1 mm, OD of 1 mm and operating pressure up to 30 MPa was connected to each ROLSI valve and suspended down into the cell. Samples were analysed using an Agilent 7890A GC coupled with a capillary column (Agilent J&W HP/PLOT-U) and a thermal conductivity detector.

GC detector calibration procedure

The pure fluids used in the VLE measurements were received directly from the suppliers listed in Table 2 and were used without further purification.

Table 2: Details of chemicals used.

ASHRAE Refrigerant Number	IUPAC name	Chemical formula	CAS #	Supplier	Mole Fraction Purity*
R744	Carbon Dioxide	CO_2	124-38-9	CoreGas	0.99995
R1243zf	3,3,3-Trifluoropropene	$C_3H_3F_3$	667-21-4	SynQuest Lab	0.99
N/A	Hydrogen	H_2	1333-74-0	BOC	0.99999

* Based on the supplier reports.

Mixtures were made for two purposes: (1) GC detector calibration and (2) VLE measurements. For the GC detector calibration, five binary mixtures of CO_2 and HFO-1243zf were prepared volumetrically, and the exact compositions were determined gravimetrically. The procedure began with weighing evacuated 300 mL Swagelok stainless steel cylinders ten times on an

electronic scale with precision up to 0.01 g. Two separate pressure, temperature and relative humidity sensors were used to capture the average ambient conditions of the measuring environment before and after weighing the cylinders to correct the measured mass for the buoyancy effect of air [38]. This process was repeated 6 hours after the first measurement to obtain an averaged value of the initial cylinder mass. The volumes of HFO-1243zf and CO_2 needed to prepare 10, 30, 50, 70, & 90 mol% of CO_2 was calculated according to the Helmholtz free energy EOS [17,39] for pure components, respectively. After pressurisation in a syringe pump (Teledyne ISCO pump 260D) for 12 hours to reach a stable pressure of 2 MPa, HFO-1243zf was injected into the empty cylinders, as shown in Figure 3. Similarly, pressurised pure CO_2 at 9 MPa in the syringe pump was injected into the cylinders to produce the required mixtures. The cylinders were weighted after each injection, as described earlier.

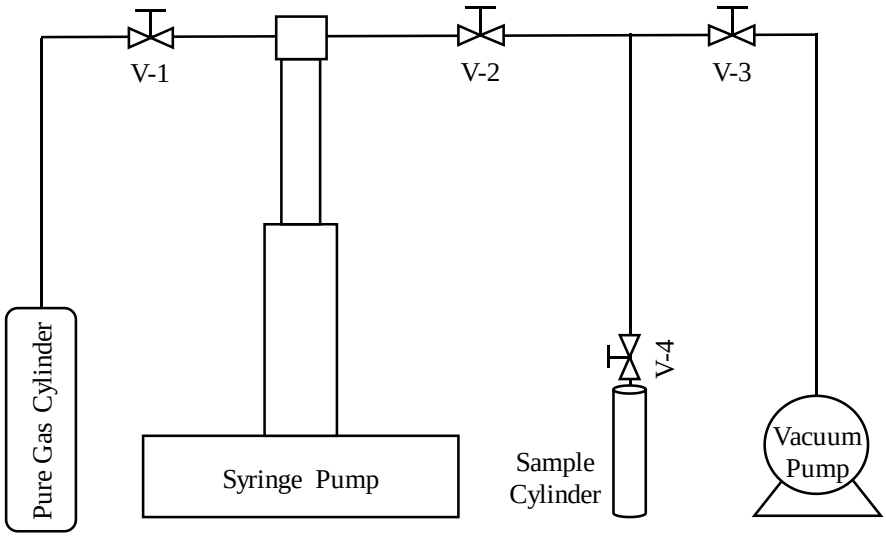

Figure 3: Gravimetric mixture preparation setup.

The mixtures prepared for GC detector calibration were transferred into the VLE measurement cell for sampling according to the following procedure: after connecting the cylinder to the equilibrium cell, all the lines were evacuated via a vacuum pump (RZ6 Vacuubrand). Then the temperature of the entire system (cell + cylinder) was increased up to 10 K higher than the cricondentherm temperature of the synthetically prepared binary mixture to ensure the mixture

was in a single-phase condition during the transfer. The bottom part of the cylinder was heated using a heating pad up to 10 K higher than the incubator temperature to ensure the homogeneity of the prepared mixture by inducing convective mixing inside the cylinder. Additionally, ball bearings were placed within the cylinder to mix the prepared binary mixture by shaking the cylinder manually 20 times before transferring the mixture into the cell.

Table 3 presents the prepared mixtures' calculated cricondentherm temperatures using REFPROP 10 software package developed by NIST [40]. Then the connecting valve between the cylinder and the cell was opened to release the one-phase mixture into the cell. After injection, the cylinder was disconnected, and the mixture in the cell was left to stabilise for about 3 h under continuous stirring before any sampling commenced.

Table 3: Gravimetrically prepared mixtures' composition, molar ratio, critical and cricondentherm temperatures calculated using REFPROP 10.

z_{CO2}	$u(z_{CO2})$	$\frac{z_{CO2}}{z_{HFO-1243z_f}}$	$u(\frac{z_{CO2}}{z_{HFO-1243zf}})$	T_c /K	$T_{cricondentherm}$ /K
0.0952	0.0007	0.1062	0.0007	378.9	378.9
0.1909	0.0007	0.2383	0.0007	377.4	377.5
0.4939	0.0006	0.9858	0.0012	367.9	368.6
0.6937	0.0003	2.284	0.0016	349.1	350.8
0.8799	0.0001	7.400	0.0038	321.7	322.6

Once the calibration mixture was at a stable pressure and temperature, at least 30 samples were acquired and analysed using three different opening times of the ROLSI valves. For a given binary mixture and within the linear range of the TCD detector, the mole fraction, z_i, can be determined by solving the following system of equations:

$$(\frac{z_i}{z_j}) = k(\frac{A_i}{A_j}) \quad (1)$$

$$z_i = 1 - \frac{1}{1 + k(\frac{A_i}{A_j})} \quad (2)$$

where A_1, and A_2 represent the integrated area for the first and second components of the binary mixture, respectively, and k stands for calibration response factor of the TCD detector. Figure 4 shows the relationships obtained between the sample's molar ratios and their corresponding area ratios ($A_{CO2}/A_{HFO\text{-}1243zf}$). Table 4 presents the optimised GC method conditions used during the measurement to separate the CO2 from HFO-1243zf peaks sufficiently.

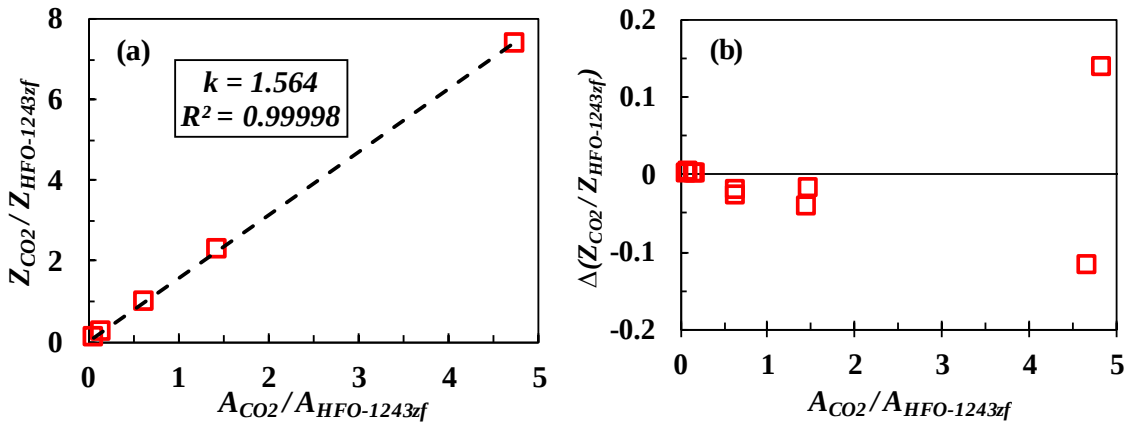

Figure 4: Thermal-conductivity detector (TCD) gravimetric calibration data CO_2 + HFO-1243zf binary system: (a) molar ratios of CO_2 to HFO-1243zf against GC area response ratios of CO_2 to HFO-1243zf, (b) deviation of molar ratios (between gravimetric determined and calculated by Equation 1) against GC area response ratios, □ experimental data, (---) Equation (1).

Table 4: The optimised GC conditions for the separation of CO_2 from HFO-1243zf.

Gas Chromatograph Parameter	Optimised Condition
Detector Conditions	
TCD temperature	443.15 K
Carrier gas	H_2
Carrier gas flow rate	15 mL/min
Makeup gas flow rate	3 mL/min
Column Conditions	
Separations column	Agilent J&W HP/PLOT-U, 320 µm D, 30 m
Oven temperature	373.15 K
Injector temperature	423.15 K
Split Ratio	100/1
CO_2 retention time	1.5 min
HFO-1243zf retention time	2.8 min

VLE measurement procedure

For the VLE measurements, the equilibrium cell and all connections were vented and evacuated before mixture preparation. A predetermined volume of HFO-1243zf was injected into the cell. The mixture's composition was then adjusted by injecting CO_2 in increments of 5 to 10% by volume to enable the majority of the phase envelope at each temperature to be covered. After each injection of CO_2, the mixture was stirred for 3 hours at the desired temperature to ensure homogeneity. When a stable pressure was reached – indicating equilibrium between vapour and liquid phases within the cell – the GC lines were flushed, and the mixture was sampled. Sampling was performed 20 times for each phase to acquire at least 10 repeatable samples.

Uncertainty analysis

The uncertainty analysis was carried out in accordance with the "Guide to the Expression of Uncertainty in Measurement (GUM)" method developed by NIST [41]. Because this study is focused on a binary system, the mole fractions *x* and *y* are defined here to represent the mole fraction of CO_2 in the liquid and vapour phases, respectively. The quantities of *T, p, x* and *y* were determined through the average of *N* independent samples acquired under almost identical measurement conditions. The standard uncertainty of the mole fraction *z* (representing either *x* or *y*) is given as follows:

$$u(z) = \sqrt{\left[\left(\frac{\partial z}{\partial T}\right)u(T)\right]^2 + \left[\left(\frac{\partial z}{\partial p}\right)u(p)\right]^2 + \left[\left(\frac{\partial z}{\partial k}\right)u(k)\right]^2 + \left[\left(\frac{\partial z}{\partial R}\right)u(R)\right]^2} \quad (3)$$

The symbols *u(T), u(p), u(k),* and *u(R)* stand for the standard uncertainty of temperature, pressure, calibration coefficient and measured peak area ratios of two components, respectively. The temperature and pressure sensors' standard uncertainties, including the uncertainties of temperature and pressure measurements, were considered to be 0.05 K and

193 0.005 MPa, respectively. The uncertainty arising from the GC detector calibration can be
194 expressed as follows:

$$u(k) = \sqrt{\left[\left(\frac{\partial k}{\partial Z_R}\right)u(Z_R)\right]^2 + \left[\left(\frac{\partial k}{\partial R}\right)u(R)\right]^2} \quad (4)$$

195 In Equation (4), $u(Z_R)$ and $u(R)$ represent the uncertainties associated with the gravimetric
196 mixture preparation (the mole ratio of CO_2 to HFO-1243zf in each calibration mixture) and
197 measured peak area response ratios during the calibration process, respectively. In Equations
198 (3) and (4), $u(R)$ is considered to be equal to the standard deviation of the measured area ratios
199 during the VLE and calibration measurements, respectively. The term $u(Z_R)$ consists of the
200 uncertainties associated with the injected masses of CO_2 and HFO-1243zf into the cylinders
201 during gravimetric mixture preparation. The standard uncertainty of the mass change recorded
202 at each weighing is based on the resolution of the scale (0.01 g). Table 3 presents the standard
203 uncertainties of the CO_2 mole fraction in the gravimetrically prepared mixtures, calculated
204 according to the method described by Arami-Niya et al. [11], which vary between 0.0001 and
205 0.0007. The mole fraction uncertainties associated with the VLE measurements are reported in
206 Table 5 and range from 0.001 to 0.008.

207 **Thermodynamic modelling**

208 The predictions of two equations of state used commonly for refrigerant mixtures, namely a
209 Helmholtz energy model and the cubic PRA EOS, were tested against the obtained
210 experimental results. The PRA EOS correlates pressure, temperature and volume as follows [42]:

$$p = \frac{RT}{v-b} - \frac{a}{v^2 + 2bv - b^2} \quad (5)$$

211 The symbol R is the universal gas constant, and v is the molar volume. Furthermore, a and b
212 stand for temperature-dependent energy and co-volume parameters, respectively. The PR-EOS

can be used for pure fluids as well as mixtures by employing, for example, the van der Waals one-fluid mixing rules that incorporate a single binary interaction parameter (BIP). A temperature-independent BIP (k_{ij}) was used in this study since the measurement temperature range was limited.

$$a = \sum_i \sum_j x_i x_j (1 - k_{ij}) \sqrt{a_i a_j} \tag{6}$$

$$b = \sum_i x_i b_i \tag{7}$$

The PRA-EOS implemented in the Multiflash software package version 7.0 was used in this study to predict the VLE property data. The PRA-EOS fits parameters of a_i and a_j in the van der Waals mixing rules to the components' vapour pressure curves over a range of reduced temperatures as follows [43]:

$$a_i = a_{ci}(1 + \kappa_{i1} t_i + \kappa_{i2} t_i^2 + \kappa_{i3} t_i^3 + \kappa_{i3} t_i^4 + \kappa_{i5} t_i^5 \tag{8}$$

$$t_i = 1 - \sqrt{\frac{T}{T_{ci}}} \tag{9}$$

Here the constants κ_{i1} to κ_{i5} are determined by the linear regression to the vapour pressure of the component *i* over a range of reduced temperatures, which corresponds to the stored vapour pressure correlation. Further information can be found in the MultiFlash user manual [43].

The BIP in Equation (6) was adjusted by regression to the experimental results measured in this work. The best-fit value k_{ij} was found by minimising the objective function of (*S*) defined as [44]:

$$S = \sqrt{\frac{1}{N}\sum_{i=1}^{N}\left[(x_{2,i} - x_{2,i,calc})^2 + (y_{2,i} - y_{2,i,calc})^2\right]} \quad (10)$$

The symbol *N* represents the total number of VLE data points used in the fitting of the EOS. The parameters $x_{2,i}$ and $x_{2,i,calc}$ stand for the experimental and predicted bubble point mole fractions of HFO-1243zf for the VLE data point "*i*". The parameters $y_{2,i}$ and $y_{2,i,calc}$ correspond to the experimental and predicted dew point mole fractions of HFO-1243zf for the same data point "*i*".

On the other hand, the Helmholtz free energy EOS are considered state-of-the-art models for predicting the thermodynamic properties of refrigerant mixtures, particularly if sufficient data are available at the time of their development. The default GERG-2008 EOS mixing rules [45], implemented in the software package NIST REFPROP 10, are shown below: these represent the reducing functions which contain BIPs used to improve the agreement between properties measured for binary mixtures and those predicted using the Helmholtz model:

$$\frac{1}{\rho_{c,ij}} = \beta_{v,ij}\gamma_{v,ij}\frac{x_i + x_j}{\beta_{v,ij}^2 x_i + x_j} \cdot \frac{1}{8}\left(\frac{1}{\rho_{c,i}^{1/3}} - \frac{1}{\rho_{c,j}^{1/3}}\right) \quad (11)$$

$$T_{c,ij} = \beta_{T,ij}\gamma_{T,ij}\frac{x_i + x_j}{\beta_{T,ij}^2 x_i + x_j} \cdot (T_{c,i}T_{c,j})^{1/2} \quad (12)$$

Here $\rho_{c,i}$, $\rho_{c,j}$, $T_{c,i}$, $T_{c,j}$, x_i and x_j are the critical density, critical temperature and mole fraction of components *i* and *j*; and the constants $\beta_{T,ij}$, $\gamma_{T,ij}$, $\beta_{v,ij}$, and $\gamma_{v,ij}$ are four independent BIPs that can be adjusted if sufficient experimental data spanning a wide range of conditions are available. If the experimental data for the binary mixture are limited, the BIPs are set to unity. In this work, only two parameters $\beta_{T,ij}$, and $\gamma_{T,ij}$ included within Equations (11) and (12) were adjusted to minimise the objective function shown in Equation (10), while the other BIPs ($\beta_{v,ij}$,

and $\gamma_{v,ij}$) were set to unity. The two tuned parameters are the most appropriate factors for fitting Helmholtz free energy EOS to VLE data, as discussed by Bell and Lemmon [46].

Results and discussion

VLE data

The VLE of CO_2 + HFO-1243zf binary system was measured at five temperatures between (288 and 348) K and pressures from (0.68 to 7.69) MPa. Table 5 presents the average of the measured temperature, pressure, relative volatility and composition of the liquid and vapour phases at each equilibrium condition. Figure 5 shows the experimental pressure and composition data, together with values calculated using the two tuned models.

Table 5: The experimental liquid (x) and vapour (y) phase mole fractions of CO_2 in binary mixtures with HFO-1243zf mixtures at equilibrium temperatures (T) and pressures (p)*.

T/K	p/MPa	x	y	α_{12}**	$u(x)$	$u(y)$	$u(\alpha_{12})$
289.6	0.680	0.0606	0.3226	7.39	0.0020	0.0080	0.38
288.9	0.861	0.1134	0.4875	7.44	0.0030	0.0074	0.31
289.3	1.127	0.1820	0.6138	7.14	0.0041	0.0066	0.28
289.2	1.428	0.2589	0.7063	6.88	0.0052	0.0057	0.27
288.9	1.851	0.3638	0.7879	6.49	0.0062	0.0045	0.25
288.7	2.305	0.4688	0.8434	6.10	0.0067	0.0036	0.23
288.5	3.146	0.6460	0.9070	5.34	0.0063	0.0023	0.21
288.5	3.612	0.7364	0.9305	4.79	0.0054	0.0018	0.19
288.5	4.012	0.8042	0.9503	4.62	0.0045	0.0014	0.19
288.9	4.291	0.8576	0.9619	4.19	0.0037	0.0011	0.18
297.3	0.688	0.0299	0.1590	6.56	0.0015	0.0071	0.29
297.1	0.938	0.0898	0.3914	6.52	0.0025	0.0073	0.28
298.2	1.276	0.1616	0.5473	6.27	0.0038	0.0069	0.25
298.2	1.669	0.2467	0.6631	6.01	0.0050	0.0061	0.23
297.3	2.099	0.3437	0.7499	5.73	0.0060	0.0050	0.22
297.3	2.665	0.4515	0.8147	5.34	0.0067	0.0040	0.20
298.2	3.398	0.5738	0.8639	4.72	0.0066	0.0032	0.18
297.3	4.205	0.7167	0.9117	4.08	0.0056	0.0022	0.16
297.3	5.151	0.8493	0.9501	3.38	0.0039	0.0014	0.14
297.4	5.660	0.9020	0.9704	3.57	0.0029	0.0010	0.17

317.7	1.140	0.0281	0.1228	4.84	0.0012	0.0051	0.32
317.8	1.514	0.0950	0.3339	4.78	0.0025	0.0064	0.19
317.8	1.804	0.1455	0.4413	4.64	0.0034	0.0068	0.18
317.8	2.257	0.2205	0.5549	4.41	0.0046	0.0066	0.17
317.7	2.876	0.3166	0.6558	4.11	0.0058	0.0060	0.16
317.7	3.604	0.4193	0.7307	3.76	0.0065	0.0053	0.14
317.8	4.392	0.5241	0.7906	3.43	0.0066	0.0045	0.13
317.7	5.647	0.6724	0.8491	2.74	0.0060	0.0035	0.10
317.8	6.927	0.8037	0.8809	1.81	0.0043	0.0028	0.07
318.2	7.651	0.8610	0.8692	1.07	0.0078	0.0104	0.12
333.4	1.905	0.0706	0.2185	3.68	0.0019	0.0052	0.16
333.5	2.239	0.1174	0.3202	3.54	0.0029	0.0061	0.14
333.4	2.666	0.1766	0.4251	3.45	0.0039	0.0066	0.13
333.5	3.197	0.2460	0.5088	3.17	0.0049	0.0067	0.12
333.4	3.724	0.3128	0.5760	2.98	0.0057	0.0065	0.11
333.6	4.380	0.3898	0.6297	2.66	0.0063	0.0062	0.10
333.6	5.357	0.4987	0.6928	2.27	0.0066	0.0057	0.09
333.4	6.437	0.6129	0.7573	1.97	0.0063	0.0049	0.07
333.3	7.693	0.7353	0.8000	1.44	0.0052	0.0043	0.05
348.3	2.307	0.0423	0.1113	2.84	0.0014	0.0035	0.14
348.2	2.228	0.0324	0.0885	2.90	0.0012	0.0032	0.16
348.2	2.863	0.1127	0.2602	2.77	0.0028	0.0054	0.11
348.2	4.031	0.2550	0.4389	2.29	0.0050	0.0067	0.09
348.1	4.644	0.3218	0.5008	2.11	0.0058	0.0067	0.08
348.1	5.326	0.3930	0.5536	1.92	0.0063	0.0066	0.07
348.2	6.145	0.4864	0.5704	1.40	0.0066	0.0065	0.05
348.5	7.112	0.6125	0.6202	1.03	0.0062	0.0062	0.04

* The standard uncertainties in temperature, *u(T)*, and pressure, *u(p)*, are 0.1 K and 0.005 MPa, respectively.

** The relative volatility of CO_2 (1) to HFO-1243zf (2) in their binary systems.

253

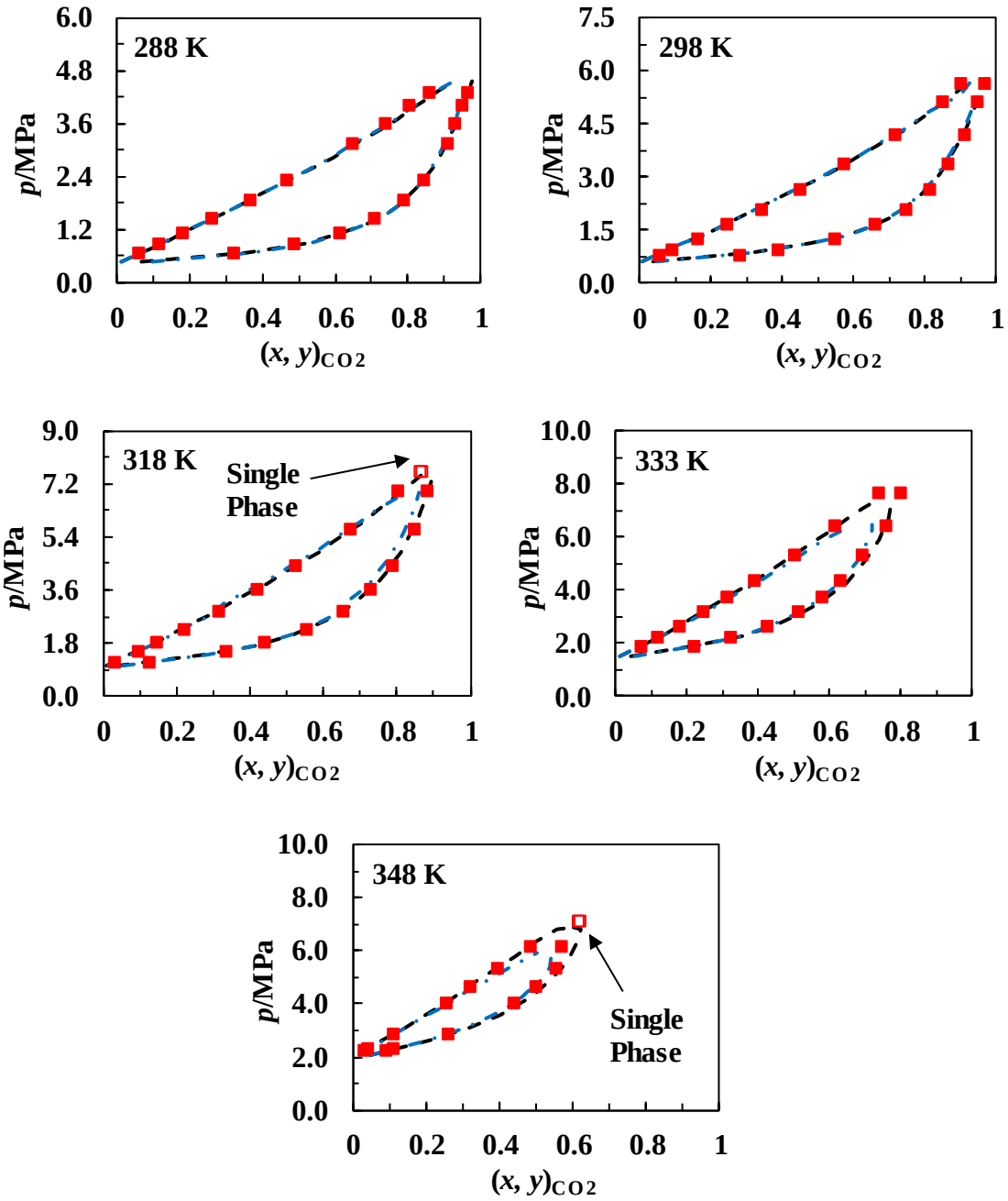

Figure 5: VLE data and calculated phase envelopes for the CO_2 + HFO-1243zf system at 288 K, 298 K, 318 K, 333 K and 348 K: (- · -) PRA-EOS (tuned); (---) Helmholtz free energy EOS (tuned); ■ this work (hollow symbols show the measured compositions in the dense phase region, acquired to check the Helmholtz energy EOS prediction of a two-phase condition).

Thermodynamic consistency and relative volatility

Figure 6 shows experimental and predicted relative volatility (α_{12}) of CO_2 to HFO-1243zf at the five temperatures between (288 and 348) K. The relative volatility of CO_2 to HFO-1243zf was decreased by increasing the overall CO_2 mole fraction and equilibrium temperature.

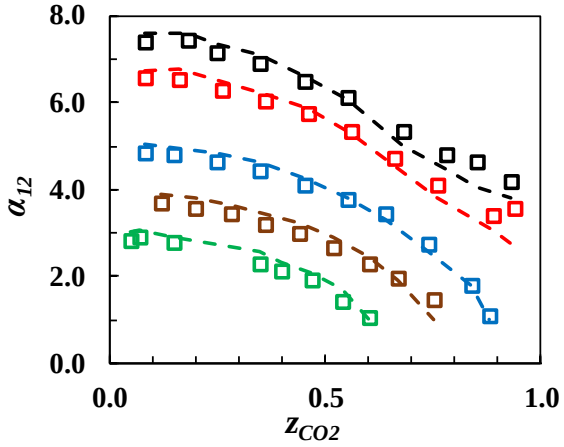

Figure 6: The relative volatility (α_{12}) of CO_2 (1) to HFO-1243zf (2) for experimental equilibrium points (□) and the predicted values by the Helmholtz Energy EOS (---); black , T = 288 K; red, T = 298 K; blue T = 318 K; brown, T = 333 K and green, T = 348 K.

The measured VLE data were assessed for thermodynamic consistency by analysing the vapour enhancement factors of HFO-1243zf for CO_2 + HFO-1243zf binary system. The enhancement factor is equal to the quotient of the experimental partial pressure of HFO-1243zf and the saturation vapour pressure of pure HFO-1243zf at the same equilibrium temperature, which is as calculated as follow:

$$f = \frac{y_{HFO-1243zf} p_{exp}}{p^{sat}_{HFO-1243zf}} \tag{13}$$

Here, the parameters $y_{\text{HFO-1243zf}}$ and p_{exp} are the measured mole fraction of HFO-1243zf in the vapour phase and the pressure of the equilibrium mixture, while $p^{sat}_{HFO-1243zf}$ is the saturation vapour pressure of HFO-1243zf at the equilibrium temperature calculated by REFPROP 10. For each isotherm, the enhancement factor will approach unity in the limit of zero equilibrium

pressure. Figure 7 shows the enhancement factor for the measure VLE data. It can be seen that all data sets are thermodynamically consistent, where the enhancement factor approaches unity at low pressures.

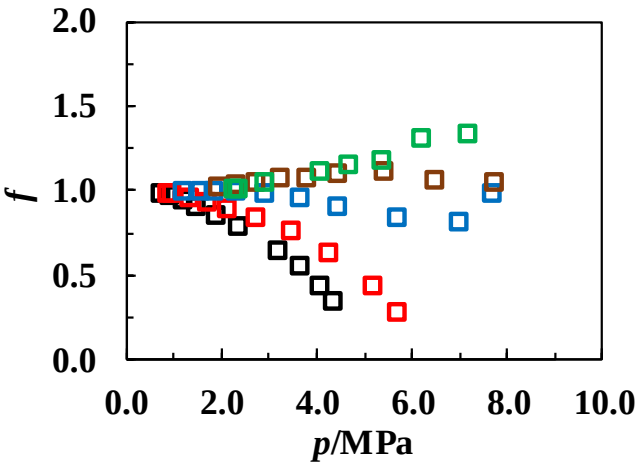

Figure 7: The enhancement factor for HFO-1243zf in CO_2 + HFO-1243zf binary system on five isotherms of 288 K (black), 298 K (red), 318 K (blue), 333 K (brown) and 348 K (green).

Model tuning

Figure 8 illustrate the differences between the experimental results and the liquid and vapour compositions predicted by the original (un-tuned) Helmholtz energy and PRA EOS. In these plots, the abscissa is the measured saturation pressure, and the ordinates are the differences between the measured and predicted mole fractions of CO_2. The mole fractions for each phase were computed by performing a flash calculation at the corresponding experimental pressure and temperature. The bulk (overall) composition of the binary mixture used as input to the flash calculation was taken to be the experimental value. Generally, the Helmholtz energy EOS provided a better representation of the VLE data than the PRA-EOS, with the deviations of both models being about 3 to 4 times larger than the experimental uncertainty. The variation between the experimental and predicted data for the bubble points increased with pressure for both models. The Helmholtz EOS provided a better representation of the dew points data at

low pressure than the PRA EOS, but at high pressure, the performance of the two models in predicting the dew point condition was reversed.

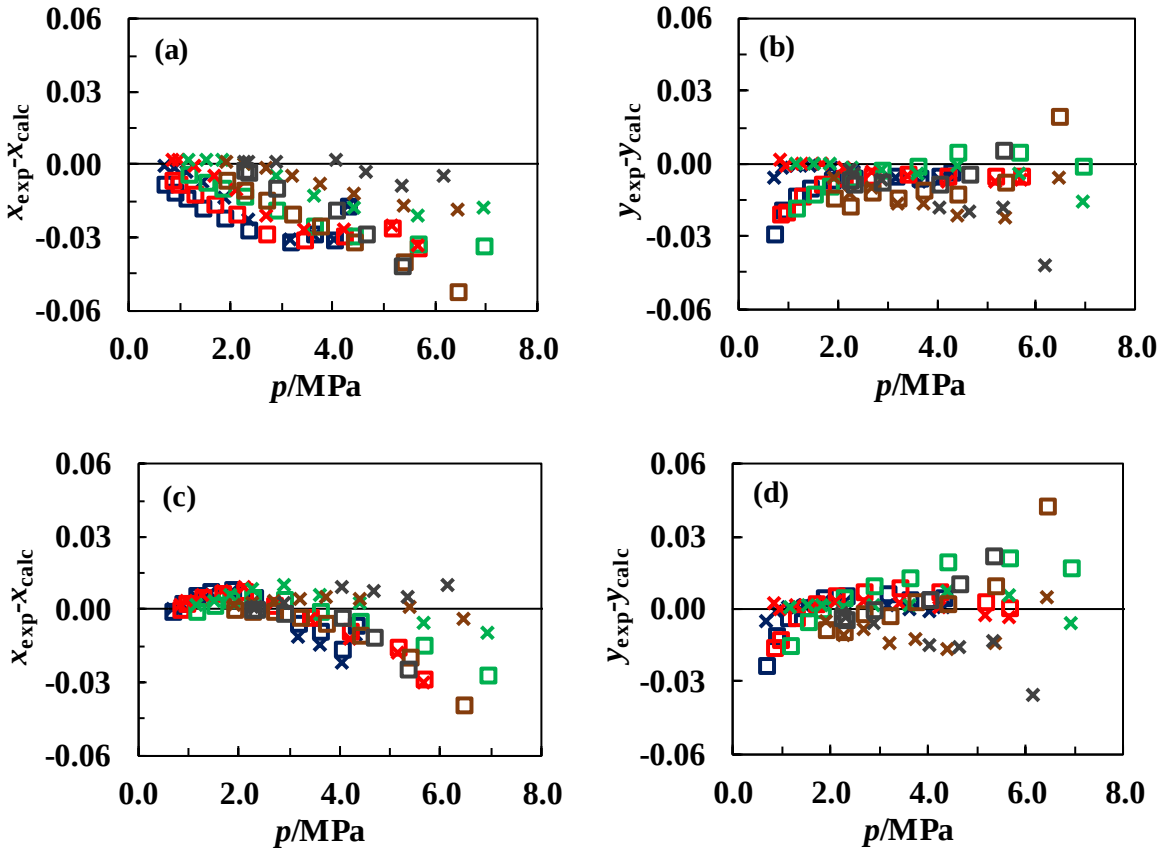

Figure 8: Absolute differences between the measured mole fraction (x_{exp}, y_{exp}) and the predicted values (x_{calc}, y_{calc}) by the original and tuned PRA-EOS (□) and Helmholtz Energy EOS (×) for the first component (CO_2); (a) bubble points – original models; (b) dew points – original models; (c) bubble point – tuned models and (d) dew points – tuned models; navy blue, T = 288 K; red, T = 298 K; green, T = 318 K; brown, T = 333 K and dark grey, T = 348 K. The average experimental uncertainty for all the experimental VLE data was a CO_2 mole fraction of 0.005.

When fitting the PRA-EOS and Helmholtz EOS binary interaction parameters, the four experimental data points acquired closest to the critical point at 318, 333 and 348 K were omitted from the regression as the models failed to follow the measured phase envelopes at those conditions. Tuning the PRA-EOS to the experimental data allowed the objective function (Equation 10) to be decreased from 0.026 with an original BIP of zero to 0.016 with an optimised BIP of k_{ij} = 0.0254. For the Helmholtz EOS, the fitted binary interaction parameters of ($\beta_{T,ij}$ = 1.009 and $\gamma_{T,ij}$ = 0.992) decreased the objective function from 0.019 to 0.012. The

final objective function for the Helmholtz EOS is more than two times of the average experimental uncertainty of 0.005 mole fraction of CO_2. This shows the reliability of the model optimisation compared with the experimental uncertainty. Figure 8 (c) and (d) show the differences between the experimental and predicted liquid and vapour compositions by the tuned Helmholtz EOS and PRA-EOS. The deviations of the bubble points decreased significantly for both models after tuning, particularly at lower pressures.

Table 6 presents RMSD and maximum deviation values for the original and tuned EOS. The tuned Helmholtz energy model represents dew and bubble points with lower RMSDs (0.009 for each phase) than the tuned PRA-EOS (0.012 for each phase). The maximum deviation between the experimental and predicted dew and bubble points by the Helmholtz free energy EOS decreased from 0.042 and 0.034 to 0.036 and 0.030, respectively, after tuning the model. The tuned PRA-EOS predicted the mole fractions for the liquid phases better than the original PRA-EOS, where the RMSDs decreased from 0.024 to 0.012. We note that the RMSD for the vapour phase increased from 0.011 to 0.012 after tuning the PRA-EOS, even though the total RMSD decreased from 0.019 to 0.012. Further optimisation of Helmholtz energy EOS would require more extensive experimental data for other properties such as density and heat capacity.

Table 6: Model deviations for the original and tuned PRA-EOS and Helmholtz free energy EOS*

Error	PRA-EOS (original)	PRA-EOS (tuned)	Helmholtz Free energy EOS (original)	Helmholtz Free energy EOS (tuned)
Total RMSD	0.019	0.012	0.013	0.009
RMSD (*y*)	0.011	0.012	0.011	0.009
RMSD (*x*)	0.024	0.012	0.015	0.009
Max. Deviation (*y*)	0.029	0.042	0.042	0.036
Max. Deviation (*x*)	0.052	0.039	0.034	0.030

* The average experimental uncertainty for all the VLE data was a CO2 mole fraction of 0.005.

Comparison between HFO-1234yf, HFO-1234ze and HFO-1243zf

In this section, the phase behaviours of three HFO candidates of replacing HFC-134a in equimolar mixtures with CO_2 were compared. Figure 9 (a) shows the phase diagrams for the binary mixtures. HFO-1234yf and HFO-1243zf binary mixtures with CO_2 have almost identical bubble pressures, while the latter has a wider liquid and vapour saturation temperatures difference for a particular equilibrium pressure. Figure 9 (b) illustrates the *p-H* diagrams for the binary mixtures. HFO-1243zf binary mixture with CO_2 have a wider liquid and vapour saturation enthalpies at a particular operating pressure compared with other HFO binaries.

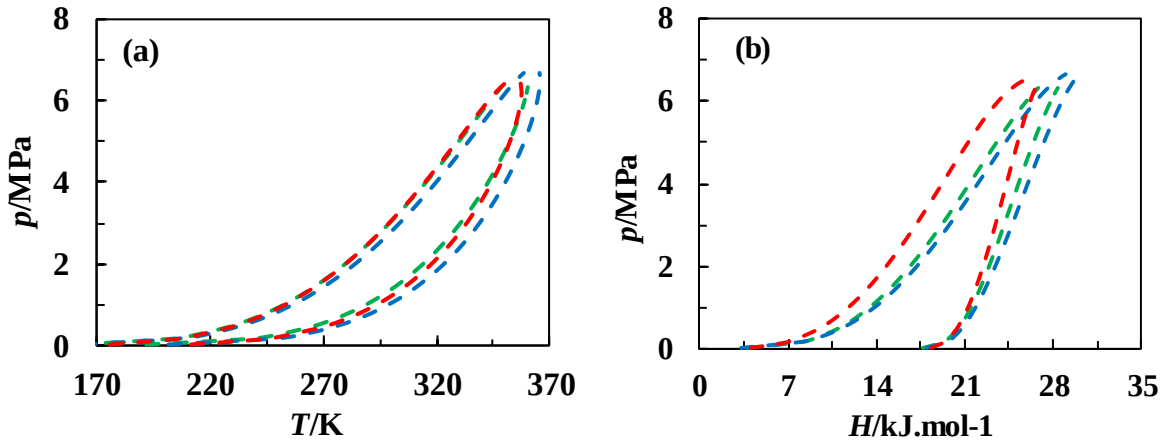

Figure 9: (a) *p-T* and (b) *p-H* diagrams of three equimolar binary mixtures of (1) CO_2 + HFO-1243zf (red), (2) CO_2 + HFO1234yf (green) and (3) CO_2 + HFO-1234ze (blue), predicted by the Helmholtz energy EOS embedded in the REFPROP 10. The model was tuned for the binary (1) based on this work and for the binaries (2) and (3) based on Arami-Niya et. [11].

Conclusions

New experimental vapour-liquid equilibrium data for CO_2 + HFO-1243zf binary mixtures are reported at temperatures from (288 to 348) K, and pressures between (0.68 and 7.69) MPa. Data presented in this work were compared with the predictions of a Helmholtz free energy model that utilises the GERG-2008 mixing rule and the Peng-Robinson Advanced EOS with

van der Waals one-fluid mixing rules. Both models' binary interaction parameters were determined by fitting to the experimental data. The PRA-EOS with the tuned binary interaction parameter provided a slightly better prediction than the original Helmholtz free energy EOS. However, the tuned Helmholtz free energy EOS represented the experimental bubble and dew points with an RMSD of 0.009, 33 % better than the tuned PRA-EOS and 45 % better than the un-tuned Helmholtz free energy EOS. The phase behaviours of three HFO candidates in equimolar mixtures with CO_2 were compared. The binary mixture studied in this work has the greatest enthalpy variation during phase change at a particular equilibrium pressure. This work provides new accurate VLE data that will aid in designing and simulating refrigeration processes utilising working fluids with low global warming potential. Further experimental thermophysical data, in particular density, should be acquired to enable further improvements in the performance of engineering models.

Acknowledgements

This research was funded by the Australian Government International Research Training Program (RTP) Scholarship for Mr Mirhadi Seyyed Sadaghiani. We thank Mr Craig Grimm for his technical assistance in the laboratory.

References

(1) Yang, Z.; Tang, X.; Wu, J.; Lu, J. Experimental Measurements of Saturated Vapor Pressure and Isothermal Vapor-Liquid Equilibria for 1,1,1,2-Tetrafluoroethane (HFC-134a) + 3,3,3-Trifluoropropene (HFO-1243zf) Binary System. *Fluid Phase Equilib.* **2019**, *498*, 86–93. https://doi.org/10.1016/J.FLUID.2019.06.020.

(2) González, S.; Jiménez, E.; Ballesteros, B.; Martínez, E.; Albaladejo, J. Hydroxyl Radical Reaction Rate Coefficients as a Function of Temperature and IR Absorption Cross Sections for CF3CH=CH2 (HFO-1243zf), Potential Replacement of CF3CH2F (HFC-134a). *Environ. Sci. Pollut. Res.* **2015**, *22* (7), 4793–4805. https://doi.org/10.1007/s11356-014-3426-2.

(3) No. 26369. Montreal Protocol on Substances That Deplete the Ozone Layer. Concluded at Montreal on 16 September 1987. **2000**, *1522* (26369), 422–447. https://doi.org/10.18356/df488915-en-fr.

(4) UNEP. The Kigali Amendment to the Montreal Protocol: HFC Phase-Down. *28th Meet. Parties to Montr. Protoc. 10-14 October, 2016, Kigali, Rwanda* **2016**, 1–7.

(5) Mylona, S. K.; Hughes, T. J.; Saeed, A. A.; Rowland, D.; Park, J.; Tsuji, T.; Tanaka, Y.; Seiki, Y.; May, E. F. Thermal Conductivity Data for Refrigerant Mixtures Containing R1234yf and R1234ze(E). *J. Chem. Thermodyn.* **2019**, *133*, 135–142. https://doi.org/10.1016/j.jct.2019.01.028.

(6) Akhfash, M.; Al Ghafri, S. Z. S.; Rowland, D.; Hughes, T. J.; Tsuji, T.; Tanaka, Y.; Seiki, Y.; May, E. F. Liquid and Vapor Viscosities of Binary Refrigerant Mixtures Containing R1234yf or R1234ze(E). *J. Chem. Eng. Data* **2019**, *64* (3), 1122–1130. https://doi.org/10.1021/acs.jced.8b01039.

(7) Al Ghafri, S. Z.; Rowland, D.; Akhfash, M.; Arami-Niya, A.; Khamphasith, M.; Xiao, X.; Tsuji, T.; Tanaka, Y.; Seiki, Y.; May, E. F.; Hughes, T. J. Thermodynamic Properties of Hydrofluoroolefin (R1234yf and R1234ze(E)) Refrigerant Mixtures: Density, Vapour-Liquid Equilibrium, and Heat Capacity Data and Modelling. *Int. J. Refrig.* **2019**, *98*, 249–260. https://doi.org/10.1016/j.ijrefrig.2018.10.027.

(8) Sampson, C. C.; Kamson, M.; Hopkins, M. G.; Stanwix, P. L.; May, E. F. Dielectric Permittivity, Polarizability and Dipole Moment of Refrigerants R1234ze(E) and R1234yf Determined Using a Microwave Re-Entrant Cavity Resonator. *J. Chem. Thermodyn.* **2019**, *128*, 148–158. https://doi.org/10.1016/j.jct.2018.07.011.

(9) Kim, D.; Yang, X.; Arami-Niya, A.; Rowland, D.; Xiao, X.; Al Ghafri, S. Z. S.; Tsuji, T.; Tanaka, Y.; Seiki, Y.; May, E. F. Thermal Conductivity Measurements of Refrigerant Mixtures Containing Hydrofluorocarbons (HFC-32, HFC-125, HFC-134a), Hydrofluoroolefins (HFO-1234yf), and Carbon Dioxide (CO2). *J. Chem. Thermodyn.* **2020**, *151*, 106248. https://doi.org/10.1016/j.jct.2020.106248.

(10) Yang, X.; Arami-Niya, A.; Xiao, X.; Kim, D.; Al Ghafri, S. Z. S.; Tsuji, T.; Tanaka, Y.; Seiki, Y.; May, E. F. Viscosity Measurements of Binary and Multicomponent Refrigerant Mixtures Containing HFC-32, HFC-125, HFC-134a, HFO-1234yf, and CO2. *J. Chem. Eng. Data* **2020**, *65* (9), 4252–4262. https://doi.org/10.1021/acs.jced.0c00228.

(11) Arami-Niya, A.; Xiao, X.; Al Ghafri, S. Z. S.; Jiao, F.; Khamphasith, M.; Sadeghi Pouya, E.; Sadaghiani, M. S.; Yang, X.; Tsuji, T.; Tanaka, Y.; Seiki, Y.; May, E. F. Measurement and Modelling of the Thermodynamic Properties of Carbon Dioxide Mixtures with HFO-1234yf, HFC-125, HFC-134a, and HFC-32: Vapour-Liquid Equilibrium, Density, and Heat Capacity. *Int. J. Refrig.* **2020**, *118*, 514–528. https://doi.org/10.1016/j.ijrefrig.2020.05.009.

(12) Di Nicola, G.; Di Nicola, C.; Arteconi, A.; Stryjek, R. PVTx Measurements of the Carbon Dioxide + 2,3,3,3-Tetrafluoroprop-1-Ene Binary System. *J. Chem. Eng. Data* **2012**, *57* (2), 450–455. https://doi.org/10.1021/je201051q.

(13) Yao, X.; Ding, L.; Dong, X.; Zhao, Y.; Wang, X.; Shen, J.; Gong, M. Experimental Measurement of Vapor-Liquid Equilibrium for 3,3,3-Trifluoropropene(R1243zf) + 1,1,1,2-Tetrafluoroethane(R134a) at Temperatures from 243.150 to 293.150 K. *Int. J. Refrig.* **2020**, *120*, 97–103. https://doi.org/10.1016/j.ijrefrig.2020.09.008.

(14) Deng, Z.; Xu, G.; Sun, S.; Zhao, Y.; Dong, X.; Gong, M. Isothermal (Vapour-Liquid) Equilibrium for the Binary {isobutane (R600a) + 3,3,3-Trifluoropropene (R1243zf)}cc System at Temperatures from 253.150 to 293.150 K. *J. Chem. Thermodyn.* **2020**, *150*, 106177. https://doi.org/10.1016/j.jct.2020.106177.

(15) Ding, L.; Yao, X.; Hou, Y.; Zhao, Y.; Dong, X.; Gong, M. Isothermal (Vapour-Liquid) Equilibrium for the Binary {3,3,3-Trifluoropropene (R1243zf) + Propane(R290)} System at Temperatures from 243.150 K to 288.150 K. *J. Chem. Thermodyn.* **2020**, *144*, 106091. https://doi.org/10.1016/j.jct.2020.106091.

(16) Lai, N. A. Thermodynamic Properties of HFO-1243zf and Their Application in Study on a Refrigeration Cycle. *Appl. Therm. Eng.* **2014**, *70* (1), 1–6.

https://doi.org/10.1016/j.applthermaleng.2014.04.042.

(17) Akasaka, R. Recent Trends in the Development of Helmholtz Energy Equations of State and Their Application to 3,3,3-Trifluoroprop-1-Ene (R-1243zf). *Sci. Technol. Built Environ.* **2016**, *22* (8), 1136–1144. https://doi.org/10.1080/23744731.2016.1208000.

(18) Akasaka, R.; Lemmon, E. W. Fundamental Equations of State for *Cis* -1,3,3,3-Tetrafluoropropene [R-1234ze(Z)] and 3,3,3-Trifluoropropene (R-1243zf). *J. Chem. Eng. Data* **2019**, *64* (11), 4679–4691. https://doi.org/10.1021/acs.jced.9b00007.

(19) Bobbo, S.; Nicola, G. Di; Zilio, C.; Brown, J. S.; Fedele, L. Low GWP Halocarbon Refrigerants: A Review of Thermophysical Properties. *International Journal of Refrigeration*. Elsevier Ltd June 2018, pp 181–201. https://doi.org/10.1016/j.ijrefrig.2018.03.027.

(20) Brown, J. S.; Zilio, C.; Cavallini, A. Thermodynamic Properties of Eight Fluorinated Olefins. *Int. J. Refrig.* **2010**, *33* (2), 235–241. https://doi.org/10.1016/j.ijrefrig.2009.04.005.

(21) Daubert, T. E.; Hutchison, G. Vapor Pressure of 18 Pure Industrial Chemicals. *AIChE Symp. Ser.* **1990**, *86* (279), 93–114.

(22) Brown, J. S.; Di Nicola, G.; Fedele, L.; Bobbo, S.; Zilio, C. Saturated Pressure Measurements of 3,3,3-Trifluoroprop-1-Ene (R1243zf) for Reduced Temperatures Ranging from 0.62 to 0.98. *Fluid Phase Equilib.* **2013**, *351*, 48–52. https://doi.org/10.1016/J.FLUID.2012.09.036.

(23) Higashi, Y.; Sakoda, N.; Islam, M. A.; Takata, Y.; Koyama, S.; Akasaka, R. Measurements of Saturation Pressures for Trifluoroethene (R1123) and 3,3,3-Trifluoropropene (R1243zf). *J. Chem. Eng. Data* **2018**, *63* (2), 417–421. https://doi.org/10.1021/acs.jced.7b00818.

(24) Higashi, Y.; Sakoda, N.; Islam, M. A.; Takata, Y.; Koyama, S.; Akasaka, R. Measurements of Saturation Pressures for Trifluoroethene (R1123) and 3,3,3-Trifluoropropene (R1243zf). *J. Chem. Eng. Data* **2018**, *63* (2), 417–421. https://doi.org/10.1021/acs.jced.7b00818.

(25) Di Nicola, G.; Steven Brown, J.; Fedele, L.; Securo, M.; Bobbo, S.; Zilio, C. Subcooled Liquid Density Measurements and PvT Measurements in the Vapor Phase for 3,3,3-Trifluoroprop-1-Ene (R1243zf). *Int. J. Refrig.* **2013**, *36* (8), 2209–2215. https://doi.org/10.1016/j.ijrefrig.2013.08.004.

(26) Raabe, G. Molecular Simulation Studies in Hydrofluoroolefine (HFO) Working Fluids and Their Blends. *Sci. Technol. Built Environ.* **2016**, *22* (8), 1077–1089. https://doi.org/10.1080/23744731.2016.1206796.

(27) Tomassetti, S.; Pierantozzi, M.; Di Nicola, G.; Polonara, F.; Brown, J. S. Vapor-Phase PvTx Measurements of Binary Blends of Cis-1,2,3,3,3-Pentafluoroprop-1-Ene + Isobutane and 3,3,3-Trifluoropropene + Isobutane. *J. Chem. Eng. Data* **2019**, *64* (2), 688–695. https://doi.org/10.1021/acs.jced.8b00921.

(28) Sadaghiani, M. S.; Arami-Niya, A.; Zhang, D.; Tsuji, T.; Tanaka, Y.; Seiki, Y.; May, E. F. Minimum Ignition Energies and Laminar Burning Velocities of Ammonia, HFO-1234yf, HFC-32 and Their Mixtures with Carbon Dioxide, HFC-125 and HFC-134a. *J. Hazard. Mater.* **2021**, *407*, 124781. https://doi.org/10.1016/j.jhazmat.2020.124781.

(29) McLinden, M. O.; Kazakov, A. F.; Steven Brown, J.; Domanski, P. A. A Thermodynamic Analysis of Refrigerants: Possibilities and Tradeoffs for Low-GWP Refrigerants. *Int. J. Refrig.* **2014**, *38* (1), 80–92. https://doi.org/10.1016/j.ijrefrig.2013.09.032.

(30) Bell, I. H.; Domanski, P. A.; McLinden, M. O.; Linteris, G. T. The Hunt for Nonflammable Refrigerant Blends to Replace R-134a. *Int. J. Refrig.* **2019**, *104*, 484–495. https://doi.org/10.1016/j.ijrefrig.2019.05.035.

(31) Wang, S.; Fauve, R.; Coquelet, C.; Valtz, A.; Houriez, C.; Artola, P. A.; Ahmar, E. El; Rousseau,

B.; Hu, H. Vapor–Liquid Equilibrium and Molecular Simulation Data for Carbon Dioxide (CO 2) + trans-1,3,3,3-Tetrafluoroprop-1-Ene (R-1234ze(E)) Mixture at Temperatures from 283.32 to 353.02 K and Pressures up to 7.6 MPa. *Int. J. Refrig.* **2019**. https://doi.org/10.1016/j.ijrefrig.2018.10.032.

(32) Juntarachat, N.; Valtz, A.; Coquelet, C.; Privat, R.; Jaubert, J. N. Experimental Measurements and Correlation of Vapor-Liquid Equilibrium and Critical Data for the CO 2 + R1234yf and CO 2 + R1234ze(E) Binary Mixtures. *Int. J. Refrig.* **2014**. https://doi.org/10.1016/j.ijrefrig.2014.09.001.

(33) Qin, Y.; Wang, Z.; Zhang, H.; Wu, Y. Investigation on Vapor Liquid Equilibrium for Strongly-Zeotropic Ternary Mixture of 2,3,3,3-Tetrafluoroprop-1-Ene (R1234yf) + Trifluoromethane (R23) + Tetrafluoromethane (R14). *Int. J. Heat Mass Transf.* **2017**, *114*, 1135–1145. https://doi.org/10.1016/j.ijheatmasstransfer.2017.06.014.

(34) May, E. F.; Guo, J. Y.; Oakley, J. H.; Hughes, T. J.; Graham, B. F.; Marsh, K. N.; Huang, S. H. Reference Quality Vapor-Liquid Equilibrium Data for the Binary Systems Methane + Ethane, + Propane, + Butane, and + 2-Methylpropane, at Temperatures from (203 to 273) K and Pressures to 9 MPa. *J. Chem. Eng. Data* **2015**, *60* (12), 3606–3620. https://doi.org/10.1021/acs.jced.5b00610.

(35) Efika, E. C.; Hoballah, R.; Li, X.; May, E. F.; Nania, M.; Sanchez-Vicente, Y.; Martin Trusler, J. P. Saturated Phase Densities of (CO2 + H2O) at Temperatures from (293 to 450) K and Pressures up to 64 MPa. *J. Chem. Thermodyn.* **2016**, *93*, 347–359. https://doi.org/10.1016/j.jct.2015.06.034.

(36) Guilbot, P.; Valtz, A.; Legendre, H.; Richon, D. Rapid On-Line Sampler-Injector: A Reliable Tool for HT-HP Sampling and on-Line GC Analysis. *Analusis* **2000**, *28* (5), 426–431. https://doi.org/10.1051/analusis:2000128.

(37) Richon, D. Method and Device for Taking Micro Samples from a Pressurized Fluid Contained in a Container. Organisation Mondiale De La Propriete Intellectuelle (Bureau International), Publication No FR2853414B1, 2003.

(38) Davis, R. S. Equation for the Determination of the Density of Moist Air (1981/91). *Metrologia* **1992**, *29* (1), 67–70. https://doi.org/10.1088/0026-1394/29/1/008.

(39) Span, R.; Wagner, W. A New Equation of State for Carbon Dioxide Covering the Fluid Region from the Triple-Point Temperature to 1100 K at Pressures up to 800 MPa. *J. Phys. Chem. Ref. Data* **1996**, *25* (6), 1509–1596. https://doi.org/10.1063/1.555991.

(40) Lemmon, E. W.; Bell, I. H.; Huber, M. L.; McLinden, M. O. NIST Standard Reference Database 23: Reference Fluid Thermodynamic and Transport Properties-REFPROP, Version 10.0; National Institute of Standards and Technology, 2018; Https://Www.Nist.Gov/Srd/Ref.

(41) Joint Committee for Guides in Metrology. Evaluation of Measurement Data - Guide to the Expression of Uncertainty in Measurement. *JCGM* **2008**, *100*, 1–116.

(42) Peng, D.-Y.; Robinson, D. B. A New Two-Constant Equation of State. *Ind. Eng. Chem. Fundam.* **1976**, *15* (1), 59–64. https://doi.org/10.1021/i160057a011.

(43) Infochem / KBC Advanced Technologies Ltd. *MultiFlash User Guide for Models and Physical Properties*; 2017.

(44) Souza, L. F. S.; Al Ghafri, S. Z. S.; Trusler, J. P. M. Measurement and Modelling of the Vapor–Liquid Equilibrium of (CO2 + CO) at Temperatures between (218.15 and 302.93) K at Pressures up to 15 MPa. *J. Chem. Thermodyn.* **2018**, *126*, 63–73. https://doi.org/10.1016/J.JCT.2018.06.022.

(45) Kunz, O.; Wagner, W. The GERG-2008 Wide-Range Equation of State for Natural Gases and

Other Mixtures: An Expansion of GERG-2004. *J. Chem. Eng. Data* **2012**, *57* (11), 3032–3091. https://doi.org/10.1021/je300655b.

(46) Bell, I. H.; Lemmon, E. W. Automatic Fitting of Binary Interaction Parameters for Multi-Fluid Helmholtz-Energy-Explicit Mixture Models. *J. Chem. Eng. Data* **2016**, *61* (11), 3752–3760. https://doi.org/10.1021/acs.jced.6b00257.